Telephone-cord instabilities in thin smectic capillaries

Paolo Biscari[1,*] and Maria Carme Calderer[2,†]
[1]*Dipartimento di Matematica, Politecnico di Milano, P. Leonardo da Vinci 32, 20133 Milano, Italy and Istituto Nazionale di Fisica della Materia, Via Ferrata 1, 27100 Pavia, Italy*
[2]*School of Mathematics, University of Minnesota, 206 Church Street SE, Minneapolis, Minnesota 55455, USA*
(Received 1 October 2004; revised manuscript received 15 February 2005; published 4 May 2005)

Telephone-cord patterns have been recently observed in smectic liquid-crystal capillaries. We analyze the effects that may induce them. As long as the capillary keeps its linear shape, we show that a nonzero chiral cholesteric pitch favors the Sm-A^*–Sm-C^* transition. However, neither the cholesteric pitch nor the presence of an intrinsic bending stress is able to give rise to a curved capillary shape. The key ingredient for the telephone-cord instability is spontaneous polarization. The free-energy minimizer of a spontaneously polarized Sm-A^* phase is attained on a planar capillary, characterized by a nonzero curvature. More interestingly, in the Sm-C^* phase the combined effect of the molecular tilt and the spontaneous polarization pushes towards a helicoidal capillary shape, with nonzero curvature and torsion.

DOI: 10.1103/PhysRevE.71.051701 PACS number(s): 61.30.Dk, 61.30.Pq, 77.84.Nh

I. INTRODUCTION

Telephone-cord instabilities in carbon films have been identified as processes which allow the material to relax its residual stress [1]. Recently, similar helicoid fibers have been observed in bent-shaped liquid crystals (the so-called *banana liquid crystals*) [2,3]. Below a direct nematic–smectic-C^* transition temperature, tilted layered domains grow into the isotropic phase by giving rise to thin helices of fixed diameter and pitch, whose tips advance at a constant speed. A central role in the peculiar domain shape choice appears to be played by the spontaneous polarization, which characterizes the banana molecules [4].

Although some nematics are polar liquids [5,6], the first well-known liquid crystals exhibiting significant spontaneous polarizations are found in the smectic-C^* phase. In this phase, the molecules are tilted with respect to the layer normal and thus break the mirror symmetry [7–9]. The local polarization vector of a smectic liquid crystal is perpendicular to the director. However, it is free to rotate in the plane orthogonal to it, thus giving a zero polarization average over one pitch. The electro-optic effects of the Sm-C^* phase emerge with the unwinding of the helix by surface stabilization and result in homogeneous spontaneous polarization throughout the sample. These homogeneous director states give rise to the ferroelectric Sm-C^* phases. For a much more detailed description of the role of polarization in liquid crystals, we refer the reader to the book by Lagerwall [10] and, more precisely, to Secs. 4.9–4.10, 5.4–5.6, 6.1–6.2, and 12.2–12.5 therein.

In this paper we analyze how polarization and chirality may influence the ground-state shapes of thin filaments. The experimental observations show that the smectic filaments grow by increasing their length, rather than by thickening their radius. Consequently, we will treat the filament radius as a fixed parameter and focus our attention on the determination of the preferred filament shape.

Our main results deal with a smectic liquid crystal endowed with a nonzero spontaneous polarization. In the Sm-A^* phase we find curved planar configurations (the capillary axis is bent with nonzero curvature) that have lower energy than straight ones. More interestingly, in the Sm-C^* phase the ground-state configuration is helicoidal. We derive analytical relations linking the radius and pitch of the ground-state shapes to the material parameters. These relations allow us to estimate the tilt angle of the Sm-C^* phase. The main issue, stemming from experimental evidence on telephone-cord instabilities and reflected in our results, is the fact that the mechanism for the capillary to decrease its energy is by bending and twisting. For other geometries, the mechanism for energy minimization may be the formation of domains [4,10]. However, domain formation is often coupled with the creation of energetically expensive boundary defects. The defect energy favors the changes in material geometry that we describe in our analysis.

The plan of the paper is as follows. In Sec. II we present and discuss the model and free-energy functional. Section III is devoted to linear capillary shapes: in it we show how a nonzero cholesteric pitch may anticipate the Sm-A–Sm-C transition. In Secs. IV and V we analyze the curved domains. In the former we prove that neither the cholesteric pitch nor the intrinsic bending stress is able to bend the axis of the smectic capillary. In the latter we determine the curved shapes induced by the spontaneous polarization. They turn out to be planar or three dimensional, depending on the Sm-A^*–Sm-C^* phase of the liquid crystal. In the concluding section we discuss the above results and test them against the experimental observations.

II. FREE-ENERGY FUNCTIONAL

We consider a liquid crystal occupying a curvilinear cylinder Ω. The domain is thus the set of points which lie within

*Electronic address: paolo.biscari@polimi.it
†Electronic address: mcc@math.umn.edu

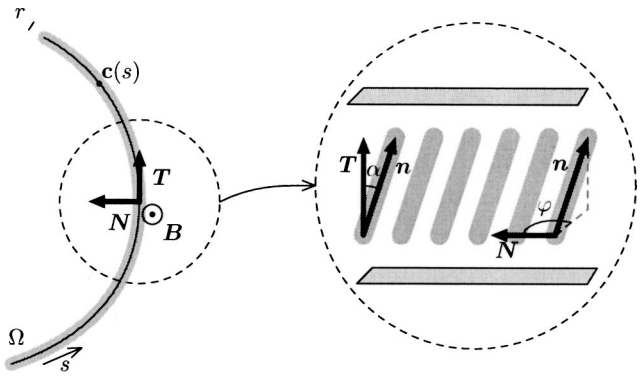

FIG. 1. Geometric setting of the model. The liquid crystal occupies a curvilinear cylinder Ω of width r, centered in the curve $\boldsymbol{c}$. The left panel illustrates the intrinsic frame $\{\boldsymbol{T},\boldsymbol{N},\boldsymbol{B}\}$. In the right enlargement we show a smectic liquid crystal, layered in the direction orthogonal to the unit tangent $\boldsymbol{T}$. The nematic director $\boldsymbol{n}$ is identified through the angles α,φ [see Eq. (2.3)].

a maximum distance r from a smooth curve $\boldsymbol{c}:[0,\ell]\to\mathbb{R}^3$ (to be determined):

$$\Omega = \{P \in \mathbb{R}^3 : P = \boldsymbol{c}(s) + \xi \boldsymbol{e}, \quad \text{for some } s \in [0,\ell], \xi \in [0,r], \quad \text{and } \boldsymbol{e}\cdot\boldsymbol{e} = 1\}. \tag{2.1}$$

Figure 1 illustrates the geometry of the problem. We let $\boldsymbol{N}$ and $\boldsymbol{B}$ be the normal and binormal unit vectors on $\boldsymbol{c}$ (the unit tangent $\boldsymbol{T}$ completes an orthogonal basis) and denote by κ and τ the curvature and torsion along the same curve. We recall that a curve characterized by constant (nonzero) values of both curvature and torsion is necessarily a cylindrical helix, whose radius and pitch are given by

$$\mathrm{r}_{\mathrm{hel}} = \frac{\kappa}{\kappa^2+\tau^2}, \quad \mathrm{p}_{\mathrm{hel}} = -\frac{2\pi\tau}{\kappa^2+\tau^2}. \tag{2.2}$$

Given a point $P \in \Omega$, the arclength $\boldsymbol{s} \in [0,\ell]$ identifies its projection on $\boldsymbol{c}$, while $\xi \in [0,r]$ yields its distance from $\boldsymbol{c}$. Finally, $\vartheta \in [0,2\pi)$ is the angle that the unit vector $\boldsymbol{e}$ in Eq. (2.1) determines with $\boldsymbol{N}$. We show in the Appendix that the coordinate set (s,ξ,ϑ) is well defined as long as Ω is sufficiently thin: $r < \min_{s\in[0,\ell]}\kappa^{-1}(s)$.

According to the experimental conditions in which smectic helices have been observed [2,3], we consider a freely suspended capillary, immersed in an isotropic fluid that does not interact with the surface director. Thus, free-boundary conditions will be imposed on both the nematic and smectic variables. However, an anchoring energy will be necessary in order to take into account the surface charges induced by spontaneous polarization.

In the absence of nematic anchoring, there is no energy gain for the system if the smectic and nematic variables depend on the transverse coordinates ξ,ϑ. We then assume throughout our calculations that all fields depend only on the arclength s. This will imply that the smectic layers are planes orthogonal to the unit tangent $\boldsymbol{T}$.

A. Nematic energy

We identify the director orientation through the angles α,φ (see Fig. 1):

$$\boldsymbol{n} = (\cos\alpha)\boldsymbol{T} + (\sin\alpha\cos\varphi)\boldsymbol{N} + (\sin\alpha\sin\varphi)\boldsymbol{B}. \tag{2.3}$$

We also introduce the unit vectors

$$\boldsymbol{n}_\perp := -(\sin\varphi)\boldsymbol{N} + (\cos\varphi)\boldsymbol{B}, \quad \boldsymbol{n}_3 := -(\sin\alpha)\boldsymbol{T} + (\cos\alpha\cos\varphi)\boldsymbol{N} + (\cos\alpha\sin\varphi)\boldsymbol{B}. \tag{2.4}$$

Together with $\boldsymbol{n}$, they complete another orthogonal basis ($\boldsymbol{n}\wedge\boldsymbol{n}_3=\boldsymbol{n}_\perp$; we arbitrarily define $\varphi=0$ when $\alpha=0$). We have (see again the Appendix for technical details)

$$\nabla\boldsymbol{n} = \left(\frac{\alpha'+\kappa\cos\varphi}{1-\kappa\xi\cos\vartheta}\boldsymbol{n}_3 + \frac{(\varphi'-\tau)\sin\alpha - \kappa\cos\alpha\sin\varphi}{1-\kappa\xi\cos\vartheta}\boldsymbol{n}_\perp\right) \otimes \boldsymbol{T},$$

where a prime denotes differentiation with respect to the arclength s. The Frank free energy density is thus given by [11]

$$\begin{aligned}\sigma_{\mathrm{F}}[\alpha,\varphi] &= K_1(\operatorname{div}\boldsymbol{n})^2 + K_2(\boldsymbol{n}\cdot\operatorname{curl}\boldsymbol{n} + q_{\mathrm{ch}})^2 + K_3|\boldsymbol{n}\wedge\operatorname{curl}\boldsymbol{n} + \boldsymbol{v}_0|^2 + (K_2+K_4)[\mathrm{tr}(\nabla\boldsymbol{n})^2 - (\operatorname{div}\boldsymbol{n})^2] \\ &= \frac{(\alpha'+\kappa\cos\varphi)^2}{(1-\kappa\xi\cos\vartheta)^2}(K_1\sin^2\alpha + K_3\cos^2\alpha) \\ &\quad + K_2\left(q_{\mathrm{ch}} - \frac{\sin\alpha}{1-\kappa\xi\cos\vartheta}\right. \\ &\quad \left.\times[(\varphi'-\tau)\sin\alpha - \kappa\cos\alpha\sin\varphi]\right)^2 + K_3\left(b_0\sin\alpha\right. \\ &\quad \left. - \frac{(\varphi'-\tau)\sin\alpha - \kappa\cos\alpha\sin\varphi}{1-\kappa\xi\cos\vartheta}\cos\alpha\right)^2,\end{aligned}$$

where q_{ch} is the cholesteric pitch and $\boldsymbol{v}_0 = b_0\boldsymbol{T}\wedge\boldsymbol{n} = b_0\sin\alpha\,\boldsymbol{n}_\perp$ is the intrinsic bending stress.

B. Smectic energy

Let $\psi(s)=\rho(s)\mathrm{e}^{i\omega(s)}$ be the smectic order parameter [11], so that

$$\nabla\psi = \frac{(\rho'+i\rho\omega')\mathrm{e}^{i\omega(s)}}{1-\kappa\xi\cos\vartheta}\boldsymbol{T},$$

and $\boldsymbol{T}$ is also the normal to the smectic layers. The smectic part of the free-energy density is given by

$$\begin{aligned}\sigma_{\mathrm{sm}}[\rho,\omega,\alpha] &= C_\parallel|\nabla\psi - iq_{\mathrm{sm}}\psi\boldsymbol{n}|^2_{\parallel n} + C_\perp|\nabla\psi - iq_{\mathrm{sm}}\psi\boldsymbol{n}|^2_{\perp n} + \zeta(\rho) = C_\parallel\left[\frac{\rho'^2\cos^2\alpha}{(1-\kappa\xi\cos\vartheta)^2}\right. \\ &\quad \left. + \rho^2\left(\frac{\omega'\cos\alpha}{1-\kappa\xi\cos\vartheta} - q_{\mathrm{sm}}\right)^2\right] \\ &\quad + \frac{C_\perp(\sin^2\alpha)(\rho'^2+\rho^2\omega'^2)}{(1-\kappa\xi\cos\vartheta)^2} + \zeta(\rho),\end{aligned} \tag{2.5}$$

where the subscript $\parallel n$ or $\perp n$ in Eq. (2.5) refers, respectively,

to the components parallel or orthogonal to the nematic director $\boldsymbol{n}$. The smectic pitch is $q_{\rm sm}$, while ζ is a scalar potential depending on the degree of smectic order.

The smectic energy (2.5) does not rule out the possibility of the elastic constants $C_\parallel, C_\perp$ being different. The $C_\perp$ term may be neglected when dealing with Sm-*A* materials [12,13], but it is necessary to keep it in the free energy when tilted phases come into play. The Sm-*A* phase may become unstable when $C_\perp < 0$ [14], and in that case a higher-order term should be included in the free energy to ensure the functional to be positive definite. However, we do not need to insert extra terms in the free energy, since we will prove that the transition to a tilted phase can be induced by the cholesteric pitch, even in the presence of a positive $C_\perp$. We remark that the free-energy density (2.5) remains positive definite even if $C_\perp$ is negative, provided α is not too large. In fact, $\sigma_{\rm sm} \geqslant 0$ whenever

$$C_\parallel \cos^2 \alpha + C_\perp \sin^2 \alpha > 0,$$

i.e.,

$$C_\perp \geqslant 0 \text{ or } \tan^2 \alpha < -\frac{C_\parallel}{C_\perp}.$$

C. Spontaneous polarization

One important difference between polar smectics and solids is the freedom of the polarization vector to rotate in the layer plane in the former ($\boldsymbol{P}$ is a Goldstone variable) as opposed to taking specific values determined by the solid lattice [10,15,16]. Because of this vectorial symmetry, the energy density of the field $\boldsymbol{P}$ contains, together with a term of the form $|\boldsymbol{\nabla P}|^2$ which penalizes interfaces in the material, a term proportional to $(\mathrm{div}\, \boldsymbol{P})^2$,

$$\sigma_{\rm pol}[\boldsymbol{P}] = G|\boldsymbol{\nabla P}|^2 + G_1(\mathrm{div}\, \boldsymbol{P})^2 + \mathcal{G}(|\boldsymbol{P}|). \qquad (2.6)$$

In Eq. (2.6), $\mathcal{G}$ denotes a scalar potential which determines the polarization intensity $|\boldsymbol{P}|$. When the permanent molecular polarization is not sufficiently strong to self-interact, this term avoids the onset of a spontaneous polarization. This is why we will insert the potential (2.6) only in Sec. V, when we will be dealing with spontaneously polarized materials.

A complete description of the polarization energy density can be found in Ref. [17]. We remark that, in materials with strong permanent polarization, the G_1 term can also take the different form $(\mathrm{div}\, \boldsymbol{P} - c_0)^2$, where c_0 can be either positive or negative. This reflects the preference of the material for a specific sign of the polarization. However, in the following we will restrict our attention to the case $c_0 = 0$. We also neglect the nonlocal Coulombian interaction of the polarization with the self-field.

D. Anchoring energy

The presence of a nonzero polarization induces a surface charge in the capillary, which in turn requires an opposite charge layer in the surrounding fluid. This boundary effect can be taken into account through an effective anchoring energy, which depends on the polarization [18,19]:

$$\sigma_{\rm anch}[\boldsymbol{P}] = \omega_P P(1 - \boldsymbol{p}\cdot\boldsymbol{\nu}),$$

where P and $\boldsymbol{p}$, respectively, denote the intensity and direction of the polarization vector $\boldsymbol{P}$, $\boldsymbol{\nu}$ is the outer normal at the external surface, and ω_P is an effective anchoring strength. The anchoring potential above may favor either homeotropic or planar anchoring for the polarization vector, depending on the sign of ω_P.

III. LINEAR SHAPES

We first consider a linear smectic capillary in the absence of spontaneous polarization. In this section we show that the presence of a nonzero cholesteric pitch may induce a Sm-*A*–Sm-*C* transition in the ground-state configuration, even if $C_\perp > 0$.

Let $\kappa = \tau \equiv 0$. The free-energy density $\sigma = \sigma_{\rm F} + \sigma_{\rm sm}$ simplifies to

$$\begin{aligned}\sigma[\alpha,\varphi,\rho,\omega] = {} & (K_1 \sin^2\alpha + K_3 \cos^2\alpha)\alpha'^2 \\ & + K_2(q_{\rm ch} - \varphi' \sin^2\alpha)^2 \\ & + K_3 \sin^2\alpha (b_0 - \varphi' \cos\alpha)^2 \\ & + C_\parallel[\rho'^2 \cos^2\alpha + \rho^2(\omega' \cos\alpha - q_{\rm sm})^2] \\ & + C_\perp \sin^2\alpha(\rho'^2 + \rho^2\omega'^2) + \zeta(\rho). \qquad (3.1)\end{aligned}$$

The Euler-Lagrange equations associated with the free-energy density (3.1), with respect to the variables φ and ω, can be easily integrated once to yield

$$\frac{\partial\sigma}{\partial\varphi'} = c_1, \quad \frac{\partial\sigma}{\partial\omega'} = c_2,$$

with c_1 and c_2 constants along the capillary. The free-boundary conditions require $c_1 = 0$ and $c_2 = 0$, and thus

$$\varphi' \equiv \frac{K_2 q_{\rm ch} + K_3 b_0 \cos\alpha}{K_2 \sin^2\alpha + K_3 \cos^2\alpha}, \quad \omega' \equiv \frac{C_\parallel q_{\rm sm} \cos\alpha}{C_\parallel \cos^2\alpha + C_\perp \sin^2\alpha}.$$

Furthermore, the free-energy density (3.1) is minimized if $\alpha' \equiv 0$ and $\rho' \equiv 0$ (which is allowed by the free-boundary conditions). When these requirements are satisfied, the free-energy density depends only on the constant values of α and ρ:

$$\begin{aligned}\sigma(\alpha_0,\rho_0) = {} & \frac{K_2 K_3 (q_{\rm ch}\cos\alpha_0 - b_0 \sin^2\alpha_0)^2}{K_2 \sin^2\alpha_0 + K_3 \cos^2\alpha_0} \\ & + \frac{C_\parallel C_\perp \rho_0^2 q_{\rm sm}^2 \sin^2\alpha_0}{C_\parallel \cos^2\alpha_0 + C_\perp \sin^2\alpha_0} + \zeta(\rho_0). \qquad (3.2)\end{aligned}$$

The smectic-*A* phase ($\alpha_0 = 0$) is always associated to a stationary point of Eq. (3.2). However, it becomes unstable even when $C_\perp > 0$, provided that

$$C_\perp q_{\rm sm}^2 \rho_0^2 < \frac{K_2}{K_3} q_{\rm ch}(K_2 q_{\rm ch} + 2 b_0 K_3). \qquad (3.3)$$

In fact,

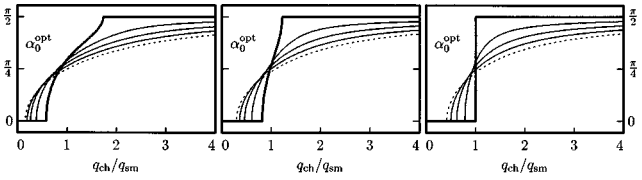

FIG. 2. α_0^{opt} as a function of $q_{\mathrm{ch}}/q_{\mathrm{sm}}$ when $K_2=K_3=C_{\parallel}\rho_0^2$; $C_{\perp}=\frac{1}{3}C_{\parallel}$ (left), $C_{\perp}=\frac{2}{3}C_{\parallel}$ (center), or $C_{\perp}=C_{\parallel}$ (right), and $b_0/q_{\mathrm{sm}}=0$ (bold line), $\frac{1}{4}$, $\frac{1}{2}$, $\frac{3}{4}$, 1 (dotted line).

$$\sigma(\alpha_0,\rho_0)=\sigma(0,\rho_0)+\left(C_{\perp}q_{\mathrm{sm}}^2\rho_0^2-\frac{K_2q_{\mathrm{ch}}(K_2q_{\mathrm{ch}}+2b_0K_3)}{K_3}\right)\alpha_0^2+O(\alpha_0^4)\quad\text{as }\alpha_0\to 0.$$

Figure 2 shows that, when condition (3.3) applies, the preferred angle moves continuously from $\alpha_0=0$. An exceptional situation arises when $b_0=0$ and $C_{\perp}=C_{\parallel}$ (bold plot of the right panel). In that case the optimal value of α_0 jumps from 0 to $\pi/2$ when q_{ch} exceeds q_{sm}. In all other cases, the Sm-A–Sm-C transition induced by the cholesteric pitch is second order.

IV. BENT DOMAINS

Let us now consider a general shape, with $\kappa,\ \tau\neq 0$, in the absence of spontaneous polarization. In this section, we prove that the combined effect of intrinsic bending stresses and/or chirality do not induce shape transitions towards curved domains.

The ground-state configuration of the free-energy density $\sigma:=\sigma_{\mathrm{F}}+\sigma_{\mathrm{sm}}$ is still characterized by $\rho'\equiv 0$ and $\omega'\equiv\text{const}$. If we further introduce the notations

$$A:=\alpha'+\kappa\cos\varphi,\quad K_{13}:=K_1\sin^2\alpha+K_3\cos^2\alpha,$$

$$\Phi:=(\varphi'-\tau)\sin\alpha-\kappa\cos\alpha\sin\varphi,\quad K_{23}:=K_2\sin^2\alpha+K_3\cos^2\alpha,$$

$$q_1:=\frac{(K_2q_{\mathrm{ch}}+K_3b_0\cos\alpha)\sin\alpha}{K_{23}},\quad q_2^2:=\frac{K_2q_{\mathrm{ch}}^2+K_3b_0^2\sin^2\alpha}{K_{23}},$$

$$\tilde{C}:=(C_{\parallel}\cos^2\alpha+C_{\perp}\sin^2\alpha)\rho_0^2,\quad \varpi:=\frac{C_{\parallel}}{\tilde{C}}\rho_0^2q_{\mathrm{sm}}\cos\alpha,$$

$$\mathcal{A}:=\pi r^2,\quad f(x):=\begin{cases}2(1-\sqrt{1-x^2})/x^2 & \text{if } x\in(0,1],\\ 1 & \text{if } x=0,\end{cases}$$

the integration of the free-energy density over the transverse coordinates yields

$$\mathcal{F}=\mathcal{A}\int_0^{\ell}ds\big[f(\kappa r)(K_{13}A^2+K_{23}\Phi^2+\tilde{C}\omega'^2)-2(K_{23}q_1\Phi+\tilde{C}\varpi\omega')+K_{23}q_2^2+C_{\parallel}\rho_0^2q_{\mathrm{sm}}^2\big].$$

The Euler-Lagrange equation for ω and the free-boundary conditions yields $\omega'\equiv\omega'_{\mathrm{opt}}=\varpi/f(\kappa r)$.

If we insert it in the free energy, we arrive at

$$\mathcal{F}=\mathcal{A}\int_0^{\ell}ds\left(f(\kappa r)(K_{13}A^2+K_{23}\Phi^2)-2K_{23}q_1\Phi+K_{23}q_2^2-\frac{\tilde{C}\varpi^2}{f(\kappa r)}+C_{\parallel}\rho_0^2q_{\mathrm{sm}}^2\right).$$

The minimum value of this energy is obtained when $\kappa=0$. To prove this assertion we notice that f is monotonically increasing.[1] In particular, it is always greater than $f(0)=1$. Furthermore, it is possible to write the free energy functional as:

$$\mathcal{F}=\mathcal{A}\int_0^{\ell}ds\left(f(\kappa r)K_{13}A^2+[f(\kappa r)-1]K_{23}\Phi^2+\tilde{C}\varpi^2\frac{f(\kappa r)-1}{f(\kappa r)}+K_{23}(\Phi-q_1)^2+\frac{K_2K_3}{K_{23}}(q_{\mathrm{ch}}\cos\alpha-b_0\sin^2\alpha)^2+\frac{C_{\parallel}C_{\perp}\rho_0^2q_{\mathrm{sm}}^2\sin^2\alpha}{C_{\parallel}\cos^2\alpha+C_{\perp}\sin^2\alpha}\right).\tag{4.1}$$

All the terms depending on the curvature [that is, all terms appearing in the first row of Eq. (4.1)] are minimized if $\kappa=0$, and thus the ground-state shape of Ω is linear. When this is the case, the search for the energy minimizer may proceed as in Sec. III.

V. POLARIZATION-INDUCED TRANSITIONS

We now focus attention on spontaneously polarized liquid crystals. First, we insert in the free-energy functional the terms σ_{pol} and σ_{anch} introduced in Sec. II. Furthermore, the intrinsic bending in the K_3 term is to be replaced by a term $\lambda\boldsymbol{P}$, proportional to the polarization vector. We will show that these changes induce a spontaneous curvature in the shape of a smectic-A^* capillary and both a curvature and a torsion in a smectic-C^* capillary.

Telephone-cord instabilities have been observed in banana liquid crystals. The microscopic shape of these molecules gives rise to a spontaneous polarization vector which is always orthogonal to the director. The vector $\boldsymbol{P}$ will thus belong to the plane determined by the unit vectors $\boldsymbol{n}_{\perp},\boldsymbol{n}_3$, defined in Eq. (2.4). We identify it through the angle ϕ as follows:

$$\boldsymbol{P}=P\boldsymbol{p}=P[(\cos\phi)\boldsymbol{n}_{\perp}+(\sin\phi)\boldsymbol{n}_3].$$

A. Bent smectic-A^* capillary

In a smectic-A phase the liquid-crystal molecules are orthogonal to the layers. We then let $\alpha\equiv 0$, which implies

[1]The function f is monotonically increasing since $f'(x)=2(2-x^2-2\sqrt{1-x^2})/(x^3\sqrt{1-x^2})>0\ \forall\ x\in(0,1)$

$$\boldsymbol{n} = \boldsymbol{T}, \quad n_\perp = \boldsymbol{B}, \quad \boldsymbol{n}_3 = \boldsymbol{N}.$$

We assume that the potentials ζ and $\mathcal{G}$ are strong enough to fix the values of $\rho \equiv \text{const} = \rho_0$ and $P \equiv \text{const} =: P_0 =: \lambda_0/\lambda$, where λ_0 has the dimensions of an inverse length.[2] In order to simplify notations, we put $\zeta(\rho_0) = \mathcal{G}(P_0) = 0$. Finally, we define $\Gamma := GP_0^2$, having the dimensions of a nematic elastic constant, and the dimensionless parameter $\gamma_1 := G_1/G$.

The bulk free-energy density $\sigma_b = \sigma_F + \sigma_{sm} + \sigma_{pol}$ now reads as

$$\sigma_b = K_2 q_{ch}^2 + K_3 \left[\left(\lambda_0 - \frac{\kappa}{1 - \kappa\xi\cos\vartheta} \right)^2 + \frac{2\kappa\lambda_0(1 - \sin\phi)}{1 - \kappa\xi\cos\vartheta} \right] + C_\parallel \rho_0^2 \left(\frac{\omega'}{1 - \kappa\xi\cos\vartheta} - q_{sm} \right)^2 + \frac{\Gamma[(\phi' + \tau)^2 + (1 + \gamma_1)\kappa^2 \sin^2\phi]}{(1 - \kappa\xi\cos\vartheta)^2}.$$

We remark that, in curved domains, the bend elastic term pushes towards configurations where the spontaneous polarization lies along the principal normal of the curve. Indeed, the K_3 term is minimized if $\sin\phi = 1$ which, together with $\alpha = 0$, implies $\boldsymbol{P} = P_0 \boldsymbol{N}$.

The anchoring energy σ_{anch} is given by

$$\sigma_{anch} = \omega_P P_0 [1 - \sin(\vartheta + \phi)].$$

If we integrate the free-energy density over the transverse section of the curve c and then we substitute the equilibrium value of ω', we finally derive the free-energy density per unit capillary length:

$$\int \sigma_{anch} r(1 - \kappa r\cos\vartheta) d\vartheta + \int\int \sigma_b \frac{\xi d\xi d\vartheta}{1 - \kappa\xi\cos\vartheta} = \mathcal{A}\ell \left[\frac{2\omega_P P_0}{r} + \kappa\omega_P P_0 \sin\phi + K_2 q_{ch}^2 + K_3[\lambda_0^2 - 2\kappa\lambda_0 \sin\phi + \kappa^2 f(\kappa r)] + C_\parallel \rho_0^2 q_{sm}^2 \frac{f(\kappa r) - 1}{f(\kappa r)} + \Gamma[(\phi' + \tau)^2 + (1 + \gamma_1)\kappa^2 \sin^2\phi] f(\kappa r) \right]. \quad (5.1)$$

To prove that the spontaneous polarization bends a smectic-A^* material, it suffices to find a curved configuration possessing a smaller free energy than the linear one. We begin by noticing that in the linear case ($\kappa = \tau = 0$) the free energy per unit length (5.1) is minimized when ϕ assumes any constant value. When this is the case, the optimal value for the free energy is

$$\mathcal{F}_{opt}|_{\kappa,\tau=0} = \mathcal{A}\ell \left(\frac{2\omega_P P_0}{r} + K_2 q_{ch}^2 + K_3 \lambda_0^2 \right). \quad (5.2)$$

We are looking for a configuration with a free energy lower than Eq. (5.2). To this aim, we focus on curves with constant curvature and torsion. The free-energy density is minimized if the polarization vector lies parallel or antiparallel to the principal normal $\boldsymbol{N}$, depending on whether K_3 is greater or smaller than $\omega_P/(2\lambda)$. In the following, we assume that $K_3 \geqslant \omega_P/(2\lambda)$. In this case the minimization process requires $\boldsymbol{p} = \boldsymbol{N}$ (i.e., $\phi = \pi/2$). Nevertheless, the considerations below would stand in the case $K_3 < \omega_P/(2\lambda)$, provided we choose $\phi = -\pi/2$.

With the choice above, the free energy depends only on the particular values chosen by κ and τ, and can be written as

$$\frac{\mathcal{F}_{opt}(\kappa,\tau)}{\mathcal{A}\ell} = A_0 - 2A_1\kappa r + A_2(\kappa r)^2 f(\kappa r) - \frac{A_3}{f(\kappa r)} + B f(\kappa r)(\tau r)^2,$$

where the signs are chosen in a way such that B and all A's are positive:

$$A_0 = K_2 q_{ch}^2 + K_3 \lambda_0^2 + C_\parallel \rho_0^2 q_{sm}^2 + 2\omega_P P_0/r,$$

$$A_1 = \left(K_3 - \frac{\omega_P}{2\lambda} \right) \frac{\lambda_0}{r},$$

$$A_2 = [K_3 + \Gamma(1 + \gamma_1)]/r^2,$$

$$A_3 = C_\parallel \rho_0^2 q_{sm}^2,$$

$$B = \Gamma/r^2.$$

The free energy $\mathcal{F}_{opt}$ is clearly minimized when $\tau = 0$ (plane curve). On the contrary, the minimum of $\mathcal{F}_{opt}$ is attained when the curvature has a strictly positive value, since

$$\frac{\mathcal{F}_{opt}(\kappa,0)}{\mathcal{A}\ell} = (A_0 - A_3) - 2A_1\kappa r + \left(A_2 + \frac{1}{3}A_3 \right)(\kappa r)^2 + O(\kappa r)^4 \quad \text{as } \kappa r \to 0.$$

We remark that $\mathcal{F}_{opt}$ possesses a unique minimum as a function of κ. Indeed, the condition $(\partial/\partial\kappa)\mathcal{F}_{opt} = 0$ is equivalent to

$$A_2[2(\kappa r) f(\kappa r) + (\kappa r)^2 f'(\kappa r)] + \frac{A_3 f'(\kappa r)}{f^2(\kappa r)} = 2A_1 \quad (5.3)$$

and this equation has one and only one root, since the function on the left-hand side vanishes when $\kappa r \to 0$, is everywhere strictly increasing and diverges when $\kappa r \to 1^-$. Let $x := \kappa r$. Equation (5.3) can be written as

$$2x f(x) + x^2 f'(x) + \xi \frac{f'(x)}{f^2(x)} = \frac{\lambda_0}{\lambda_0^*}, \quad (5.4)$$

with

[2] All the instabilities we find in this section hold also if we take into account either nonuniform P, ρ, or spontaneous polarizations not necessarily orthogonal to the director. However, we skip those quite longer proofs to shorten our presentation.

$$\xi := \frac{A_3}{A_2} = \frac{C_\parallel \rho_0^2 q_{\mathrm{sm}}^2 r^2}{K_3 + \Gamma(1+\gamma_1)}, \quad \lambda_0^* := \frac{A_2 \lambda_0}{2A_1} = \frac{K_3 + \Gamma(1+\gamma_1)}{(2K_3 - \omega_P/\lambda) r}. \tag{5.5}$$

Figure 3 shows how the solutions of Eq. (5.4) depend on λ_0 (which is proportional to the intensity of the spontaneous polarization) for three different values of the dimensionless parameter ξ. In the absence of spontaneous polarization the curvature is null. Then, it increases monotonically with λ_0. When the spontaneous polarization makes λ_0 much greater than its reference value λ_0^*, the curvature approaches its maximum allowed value r^{-1}. The curvature increases more rapidly when ξ is small—that is, in thinner capillaries.

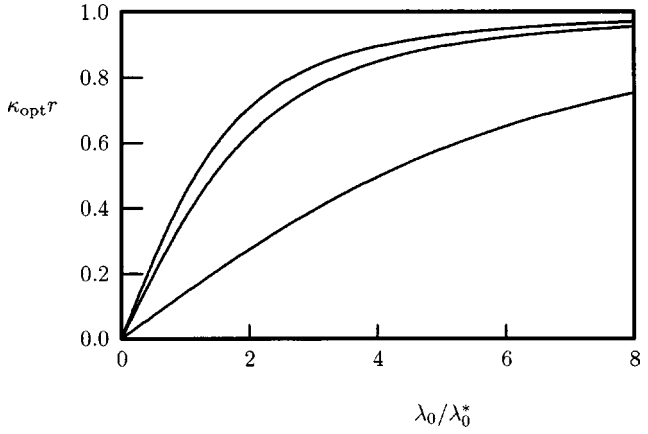

FIG. 3. The preferred curvature of the axis of the smectic-A^* capillary increases with the spontaneous polarization. The inverse length λ_0 is proportional to $|\boldsymbol{P}|$, and its reference value λ_0^* is defined in Eq. (5.5). From top to bottom, the graphs correspond to $\xi = 0, 1, 10$.

B. Helicoidal smectic-C^* capillary

In this final section we study how the spontaneous polarization may induce a telephone-cord transition in a smectic-C^* capillary. We focus on a particular, even if quite common, case. We assume that the smectic part of the free energy is able to fix the opening angle of the smectic-C^* cones to a fixed value: $\alpha \equiv \alpha_0$. Furthermore, we assume that the spontaneous polarization of the liquid-crystal molecules determines a constant angle with respect to the principal normal of the capillary ($\phi \equiv$ const).

Even under the above simplifying assumptions, the bulk free-energy density to be minimized is still quite cumbersome to handle:

$$\begin{aligned}
\sigma_{\mathrm{b}} = {} & \sigma_{\mathrm{sm}}(\alpha_0) + K_1 \frac{\kappa^2 \cos^2\varphi \sin^2\alpha_0}{(1-\kappa\xi\cos\vartheta)^2} + K_2 \left(q_{\mathrm{ch}} - \frac{\sin\alpha_0}{1-\kappa\xi\cos\vartheta}[(\varphi'-\tau)\sin\alpha_0 - \kappa\cos\alpha_0\sin\varphi] \right)^2 \\
& + K_3 \left[\left(\lambda_0 \sin\phi - \frac{\kappa\cos\varphi\cos\alpha_0}{1-\kappa\xi\cos\vartheta} \right)^2 + \left(\lambda_0\cos\phi - \frac{(\varphi'-\tau)\sin\alpha_0 - \kappa\cos\alpha_0\sin\varphi}{1-\kappa\xi\cos\vartheta}\cos\alpha_0 \right)^2 \right] \\
& + \frac{\Gamma}{(1-\kappa\xi\cos\vartheta)^2} (\{[(\varphi'-\tau)\sin\alpha_0\cos\phi + \kappa\cos\varphi\sin\phi - \kappa\cos\alpha_0\sin\varphi\cos\phi]^2 \\
& + [(\varphi'-\tau)\cos\alpha_0 + \kappa\sin\alpha_0\sin\varphi]^2\} + \gamma_1\{-[(\varphi'-\tau)\sin\alpha_0\cos\phi + \kappa\cos\varphi\sin\phi - \kappa\cos\alpha_0\sin\varphi\cos\phi]\cos\alpha_0 \\
& + [(\varphi'-\tau)\cos\alpha_0 + \kappa\sin\alpha_0\sin\varphi]\cos\phi\sin\alpha_0\}^2),
\end{aligned}$$

where σ_{sm} represents the smectic part, which fixes the value of α_0. The above expression simplifies if we introduce the quantities $\boldsymbol{x} := \{x_i, i=1,2,3\}$, $\boldsymbol{A} := \{A_{ij} : i,j = 1,2,3\}$, $\boldsymbol{b} := \{b_i, i=1,2,3\}$, and $c \in \mathbb{R}$, defined as

$$x_1 := \frac{\kappa\cos\varphi}{1-\kappa\xi\cos\vartheta}, \quad x_2 := \frac{(\varphi'-\tau)\sin\alpha_0 - \kappa\cos\alpha_0\sin\varphi}{1-\kappa\xi\cos\vartheta},$$

$$x_3 := \frac{(\varphi'-\tau)\cos\alpha_0 + \kappa\sin\alpha_0\sin\varphi}{1-\kappa\xi\cos\vartheta},$$

$$A_{11} := K_1\sin^2\alpha_0 + K_3\cos^2\alpha_0 + \Gamma(1+\gamma_1\cos^2\alpha_0)\sin^2\phi,$$

$$A_{22} := K_2\sin^2\alpha_0 + K_3\cos^2\alpha_0 + \Gamma(1+\gamma_1\cos^2\alpha_0)\cos^2\phi,$$

$$A_{33} := \Gamma(1+\gamma_1\sin^2\alpha_0\cos^2\phi),$$

$$A_{12} = A_{21} := \Gamma(1+\gamma_1\cos^2\alpha_0)\sin\phi\cos\phi,$$

$$A_{13} = A_{31} := -\Gamma\gamma_1\sin\alpha_0\cos\alpha_0\sin\phi\cos\phi,$$

$$A_{23} = A_{32} := -\Gamma\gamma_1\sin\alpha_0\cos\alpha_0\cos^2\phi,$$

$$b_1 := K_3\lambda_0\sin\phi\cos\alpha_0, \quad b_2 := K_2 q_{\mathrm{ch}}\sin\alpha_0 + K_3\lambda_0\cos\phi\cos\alpha_0, \quad b_3 := 0,$$

$$c := \sigma_{\mathrm{sm}}(\alpha_0) + K_2 q_{\mathrm{ch}}^2 + K_3\lambda_0^2$$

which allow us to write

$$\sigma_{\mathrm{b}} = \boldsymbol{x}\cdot\boldsymbol{A}\boldsymbol{x} - 2\boldsymbol{b}\cdot\boldsymbol{x} + c.$$

The scalar product between the polarization direction and the outside normal to $\partial\Omega$ is

$$\boldsymbol{p}\cdot\boldsymbol{\nu}=\cos\alpha_0\sin\phi\cos(\vartheta-\varphi)+\cos\phi\sin(\vartheta-\varphi).$$

Thus, the integration of the anchoring energy across the section orthogonal to the axis of the capillary yields

$$\int_0^{2\pi}\sigma_{\mathrm{anch}}r(1-\kappa r\cos\vartheta)d\vartheta$$

$$=\mathcal{A}[2+\kappa r(\cos\alpha_0\sin\phi\cos\varphi+\cos\phi\sin\varphi)]\frac{\omega_P P_0}{r}.$$

We now specialize our study to the small-curvature (or thin- capillary) regime $\kappa r\ll 1$. In this case we can neglect the correction to 1 in the denominators of the x_i's, and the integration of the bulk free-energy density over the transverse section simply corresponds to a multiplication by $\mathcal{A}$. This allows us to derive an analytic expression for the free-energy minimizer. In fact, in this case the total free energy can be written as

$$\frac{\mathcal{F}}{\mathcal{A}\ell}=\boldsymbol{x}\cdot\boldsymbol{A}\boldsymbol{x}-2\tilde{\boldsymbol{b}}\cdot\boldsymbol{x}+\tilde{c}, \tag{5.6}$$

provided we define the $\tilde{b}_i$'s and $\tilde{c}$ as follows:

$$\tilde{b}_1 \coloneqq \left(K_3-\frac{\omega_P}{2\lambda}\right)\lambda_0\sin\phi\cos\alpha_0,$$

$$\tilde{b}_2 \coloneqq K_2 q_{\mathrm{ch}}\sin\alpha_0+\left(K_3-\frac{\omega_P}{2\lambda}\right)\lambda_0\cos\phi\cos\alpha_0,$$

$$\tilde{b}_3 \coloneqq \frac{\omega_P P_0}{2}\cos\phi\sin\alpha_0,$$

$$\tilde{c} \coloneqq \sigma_{\mathrm{sm}}(\alpha_0)+K_2 q_{\mathrm{ch}}^2+K_3\lambda_0^2+\frac{2\omega_P P_0}{r}.$$

The functional (5.6) is minimized with respect to the possible values assumed by the x_i's when

$$\boldsymbol{x}=\boldsymbol{x}_{\mathrm{opt}}\coloneqq\boldsymbol{A}^{-1}\tilde{\boldsymbol{b}}. \tag{5.7}$$

(The symmetric matrix $\boldsymbol{A}$ is positive definite because of the positivity of the elastic free energy density.) When this is the case, the free energy takes the value

$$\frac{\mathcal{F}_{\mathrm{opt}}}{\mathcal{A}\ell}=\tilde{c}-\tilde{\boldsymbol{b}}\cdot\boldsymbol{A}^{-1}\tilde{\boldsymbol{b}}. \tag{5.8}$$

The x_i's obtained from Eq. (5.7) fix the constant values of φ, κ, and τ. Indeed, in the thin-capillary limit $\kappa r\ll 1$, and setting $\varphi'=0$, the definition of the x_i's can be written as

$$x_{\mathrm{opt},1}=\kappa\cos\varphi,$$

$$x_{\mathrm{opt},2}=-\tau\sin\alpha_0-\kappa\cos\alpha_0\sin\varphi,$$

$$x_{\mathrm{opt},3}=-\tau\cos\alpha_0+\kappa\sin\alpha_0\sin\varphi,$$

which can be inverted to obtain

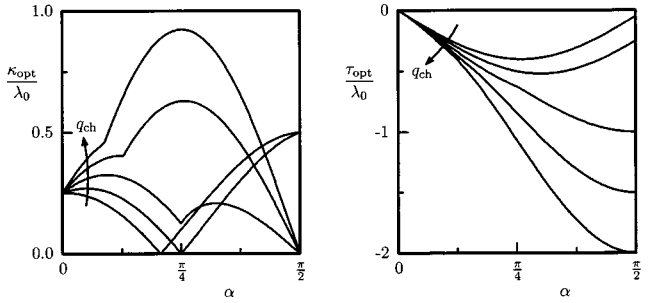

FIG. 4. Curvature and torsion of an optimal-shaped smectic-C^* capillary. The plots correspond to the values $q_{\mathrm{ch}}/\lambda_0=0.1,0.5,1.0,1.5,2$.

$$\kappa=\sqrt{x_{\mathrm{opt},1}^2+(x_{\mathrm{opt},3}\sin\alpha_0-x_{\mathrm{opt},2}\cos\alpha_0)^2},$$

$$\tau=-(x_{\mathrm{opt},2}\sin\alpha_0+x_{\mathrm{opt},3}\cos\alpha_0),$$

$$\varphi=\arctan\frac{x_{\mathrm{opt},3}\sin\alpha_0-x_{\mathrm{opt},2}\cos\alpha_0}{x_{\mathrm{opt},1}}.$$

However, at this stage, $\mathcal{F}_{\mathrm{opt}}$ in Eq. (5.8) still depends on the constant value attained by ϕ, the angle that identifies the polarization direction. Only the minimization of $\mathcal{F}_{\mathrm{opt}}$ with respect to ϕ yields the complete description of the ground-state configuration.

In order to illustrate the result of this minimization procedure we conclude this section by analyzing in detail two particular cases. In both of them the optimal shape of the smectic capillary turns out to be a three-dimensional helix, characterized by non-null values of both the curvature and torsion of its axis.

1. One-constant approximation

Let us first consider the particular case in which

$$K_1=K_2=K_3=\Gamma=\omega_P/\lambda\coloneqq K,\quad \gamma_1=0, \tag{5.9}$$

while keeping the thin-capillary regime $\lambda_0 r\ll 1$. The optimal shape of the capillary axis depends on the tilt angle α_0 of the smectic-C^* molecules and on the cholesteric pitch q_{ch}. Figure 4 illustrates the results. The right panel (displaying the torsion) proves the three-dimensional character of the capillary axis. The torsion is enhanced by the presence of a cholesteric pitch. However, a nonzero q_{ch} is not a necessary ingredient to obtain three-dimensional shapes. In fact, if we add $q_{\mathrm{ch}}=0$ to Eq. (5.9), we can derive an analytical expression for the optimal shape for all values of α_0:

$$\kappa_{\mathrm{opt}}\big|_{q_{\mathrm{ch}}=0}=\frac{|3\cos 2\alpha_0-1|}{8}\lambda_0,\qquad \tau_{\mathrm{opt}}\big|_{q_{\mathrm{ch}}=0}=-\frac{3}{8}\sin 2\alpha_0\lambda_0. \tag{5.10}$$

On the contrary, the role played by λ_0 (i.e., the spontaneous polarization) is crucial. The ratio between either κ, τ, and λ_0 is finite. Thus, both κ and τ vanish when λ_0 does so. This observation is consistent with the results presented in Sec. IV, where we have proved that the optimal capillary shape is linear if the spontaneous polarization is null. Figure 4 is also

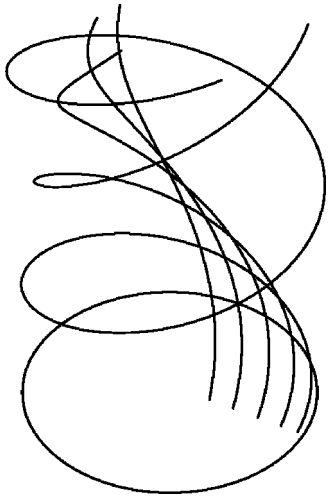

FIG. 5. Equilibrium capillary shapes for an achiral ($q_{\mathrm{ch}}=0$) Sm-C^*k, in the one-constant approximation. The plots correspond to helices whose radius and pitch are given by Eq. (5.11) for several values of the tilt angle α_0. The base circle pictures the planar equilibrium shape of a Sm-A^* ($\alpha_0=0$). As soon as $\alpha_0>0$, the circle becomes a tightly wound helix. When α_0 increases, the helix opens. The displayed shapes correspond to $\alpha_0=0°$, 5°, 10°, 15°, 20°, and 25°.

coherent with the result derived in Sec. V A for a smectic-A^* material: in the limit $\alpha\to 0$, the torsion vanishes while the curvature does not. The radius and pitch of the helical shape predicted by Eq. (5.10) are given by

$$r_{\mathrm{hel}}\big|_{q_{\mathrm{ch}}=0}=\frac{4|3\cos 2\alpha_0-1|}{5-3\cos 2\alpha_0}\lambda_0^{-1},$$

$$p_{\mathrm{hel}}\big|_{q_{\mathrm{ch}}=0}=\frac{24\pi\sin 2\alpha_0}{5-3\cos 2\alpha_0}\lambda_0^{-1}. \tag{5.11}$$

The helix pitch vanishes when α_0 vanishes, or it is equal to $\pi/2$, that is, when the director is parallel or orthogonal to the layer normal. In both cases, the equilibrium shape is a planar circle. It attains its maximum value when $\alpha_0=\frac{1}{2}\arccos\frac{3}{5}\doteq 27°$. The helix radius decreases when α_0 increases, until it vanishes at the critical value $\alpha_0=\frac{1}{2}\arccos\frac{1}{3}\doteq 35°$, where the helix becomes a linear segment. Figure 5 pictures the unwinding of the helix induced by the tilt angle α_0.

2. Small tilt angle

Let us now analyze in more detail the small-α_0 limit. If the bend elastic constant prevails again over the effective anchoring $[K_3\geqslant\omega_P/(2\lambda)]$, we obtain

$$\kappa_{\mathrm{opt}}=\frac{K_3-\omega_P/(2\lambda)}{K_3+\Gamma(1+\gamma_1)}\lambda_0+O(\alpha_0),$$

$$\tau_{\mathrm{opt}}=-\frac{K_3}{\Gamma}\left(1-\frac{K_3-\omega_P/(2\lambda)}{K_3+\Gamma(1+\gamma_1)}\right)\lambda_0\alpha_0+O(\alpha_0^2),\quad \text{as } \alpha_0\to 0.$$

These results display the same qualitative features of the one-constant solution analyzed above. The preferred curvature becomes different from zero as soon as the spontaneous polarization appears, even when α_0 vanishes. On the contrary, the torsion vanishes when either λ_0 or α_0 do so. However, a new and interesting result stems from the computation of the optimal free energy up to $O(\alpha^2)$. We obtain

$$\frac{\mathcal{F}_{\mathrm{opt}}}{\mathcal{A}\ell}=\sigma_{\mathrm{sm}}(\alpha_0)+\left[K_3\lambda_0^2-\frac{\left(K_3-\frac{\omega_P}{2\lambda}\right)^2\lambda_0^2}{K_3+\Gamma(1+\gamma_1)}+K_2q_{\mathrm{ch}}^2+\frac{2\omega_P\lambda_0}{\lambda r}\right]$$
$$-\frac{2K_2\left(K_3-\frac{\omega_P}{2\lambda}\right)\lambda_0 q_{\mathrm{ch}}\alpha_0}{K_3+\Gamma(1+\gamma_1)}+O(\alpha_0^2). \tag{5.12}$$

The minus sign in front of the first-order term in $\mathcal{F}_{\mathrm{opt}}$ is crucial. It implies that it is possible to decrease the free energy by tilting the director with respect to the layer normal. This result holds even if $\sigma_{\mathrm{sm}}(\alpha_0)$ pushes towards the smectic-A state, because in that case σ_{sm} is minimum when $\alpha_0=0$, so that it does not contribute to the $O(\alpha_0)$ term we are discussing. The structure of the first-order term in α_0 shows that this instabilization of the smectic-A^* phase is a combined effect of both the spontaneous polarization and the cholesteric pitch. Once α_0 becomes non-null, a nonzero value of the torsion becomes preferred and the ground-state configuration of the smectic-C^* phase becomes helicoidal.

VI. DISCUSSION

A. Analytical results

The present theoretical study proves that telephone-cord instabilities are to be expected in smectic-C^* liquid crystals. We have derived the ground-state configurations and the preferred shapes of a thin smectic capillary, possibly endowed with spontaneous polarization. Having in mind the experimental conditions in which these instabilities have been already observed, we have imposed free-boundary conditions at the external surface of the capillary for both the nematic and smectic variables. Nevertheless, a boundary energy has been inserted in the free-energy functional to take into account polarization effects on the surrounding liquid.

As long as the spontaneous polarization is absent, the preferred capillary shape remains linear, as we prove in Sec. IV. In this case, our analysis (Sec. III) proves that a non-null cholesteric pitch may induce a Sm-A–Sm-C transition, even if the elastic constant $C_\perp$ is positive. Figure 2 shows how the optimal value of the tilt angle α depends on the cholesteric pitch for several different values of the elastic constants and the intrinsic bending stress.

In Sec. V we have focused on spontaneously polarized smectic liquid crystals. We have found evidence for possible circular smectic-A^* and helicoidal smectic-C^* capillaries. Figure 3 shows how the curvature of a smectic-A^* capillary is expected to increase with the spontaneous polarization. Figure 4 displays both the curvature and the torsion as a function of the tilt angle, for several different values of the cholesteric pitch (which, however, turns out to be not a key ingredient in the telephone-cord transition).

In our opinion, the result derived in the final subsection, Sec. V B 2, is particularly challenging. Equation (5.12) shows that even when the smectic part of the free-energy functional pushes towards the smectic-*A* phase, it is possible to save free energy by slightly tilting the nematic molecules with respect to the layers. Once the molecules are tilted ($\alpha_0 > 0$), the preferred torsion becomes non-null, and a telephone-cord instability originates. This effect arises from a combined action of the spontaneous polarization and the cholesteric pitch.

B. Comparison with experimental measurements

The analytical predictions above can be tested against the experimental observations that inspired the present work. More precisely, the geometry we have considered closely matches the measurements carried out by the Kent and Halle groups on 2-nitro-1-3-phenylene bis [20,2]. This compound is achiral and undergoes a direct isotropic-B_7 phase transition at 177 °C. The B_7 phase is a tilted smectic phase, whose detailed structure is still under study [21,22].

The comparison between our theoretical predictions and the experimental observations of Ref. [2] allow to derive some information on the B_7 phase of the banana liquid crystal compound. More precisely, from the helical parameters we can estimate the tilting angle of the smectic phase and the polarization-induced intrinsic bend. The experimental observations evidence a capillary of radius $r = 0.85\ \mu$m, which forms a helix of radius $r_{\mathrm{hel}} = 2.25\ \mu$m and pitch $p_{\mathrm{hel}} = 6.7\ \mu$m. In the absence of more precise information on the elastic constants of the banana compound, we now assume that the one-constant approximation (5.9) holds, at least as a first-order approximation. If this is the case and considering that achirality implies $q_{\mathrm{ch}} = 0$, Eqs. (5.11) provide an estimate for both r_{hel} and p_{hel} in terms of the tilt angle α_0 and the polarization-induced intrinsic bend λ_0. The inversion of these equations leads to the estimates

$$\alpha_0 \approx 20\,^\circ, \quad \lambda_0 = \lambda P_0 \approx 1.93\ \mu\mathrm{m}^{-1}.$$

Note added in proof. Recently, we became aware of a previous paper by Sones *et al.* [23] in which a related problem was analyzed. In [23], the polarization free-energy density (2.6) was neglected and, as a consequence, the polarization vector was allowed to develop a line disclination inside the thin capillary. In that case, two instabilities can arise, depending on the value of the cholesteric pitch: an helical disclination may develop inside a straight capillary, or the capillary itself may undergo a twisting transition.

ACKNOWLEDGMENTS

This work has been supported by the NSF Contract No. DMS-0128832, "Mathematical Modeling of Advanced Liquid Crystal Materials: Ferroelectricity and Chirality." P.B. acknowledges the hospitality of the University of Minnesota, where part of this work was carried out. Some of the analytical computations and figures presented in this paper were performed with the aid of Mathematica, 5.0, licence: L4596-4499.

APPENDIX: CYLINDRICAL-CURVILINEAR COORDINATES

Let Ω be the domain defined in Eq. (2.1), $\{\boldsymbol{T},\boldsymbol{N},\boldsymbol{B}\}$ the intrinsic frame associated with $\boldsymbol{c}$, and (s,ξ,ϑ) the coordinates introduced in Eq. (2.1). Let further e_ξ, e_ϑ be the unit vectors defined as

$$\boldsymbol{e}_\xi := \cos\vartheta\boldsymbol{N} + \sin\vartheta\boldsymbol{B}, \quad \boldsymbol{e}_\vartheta := -\sin\vartheta\boldsymbol{N} + \cos\vartheta\boldsymbol{B}.$$

When we follow the intrinsic unit vectors' variation along a curve $(s(t),\xi(t),\vartheta(t))$ in Ω, the Frenet-Serret formulas imply $\dot{\boldsymbol{T}} = \kappa\dot{s}\boldsymbol{N}$, $\dot{\boldsymbol{N}} = -\kappa\dot{s}\boldsymbol{T} - \tau\dot{s}\boldsymbol{B}$, and $\dot{\boldsymbol{B}} = \tau\dot{s}\boldsymbol{N}$, so that

$$\dot{\boldsymbol{e}}_\xi = (\dot{\vartheta} - \tau\dot{s})\boldsymbol{e}_\vartheta - \kappa\dot{s}\cos\vartheta\boldsymbol{T}, \quad \dot{\boldsymbol{e}}_\vartheta = -(\dot{\vartheta} - \tau\dot{s})\boldsymbol{e}_\xi + \kappa\dot{s}\sin\vartheta\boldsymbol{T}.$$

We thus obtain

$$\dot{P} = \frac{d}{dt}[\boldsymbol{c}(s) + \xi\boldsymbol{e}_\xi] = (1 - \kappa\xi\cos\vartheta)\dot{s}\boldsymbol{T} + \dot{\xi}\boldsymbol{e}_\xi + \xi(\dot{\vartheta} - \tau\dot{s})\boldsymbol{e}_\vartheta.$$

For any differentiable real function $\Psi:\mathbb{R}^3 \to \mathbb{R}$ we have

$$\boldsymbol{\nabla}\Psi = \frac{\Psi_{,s} + \tau\Psi_{,\vartheta}}{1 - \kappa\xi\cos\vartheta}\boldsymbol{T} + \Psi_{,\xi}\boldsymbol{e}_\xi + \frac{\Psi_{,\vartheta}}{\xi}\boldsymbol{e}_\vartheta,$$

where a comma denotes differentiation with respect to the indicated variable. In particular, if Ψ depends only on the arclength s,

$$\boldsymbol{\nabla}\Psi(s) = \frac{1}{1 - \kappa\xi\cos\vartheta}\frac{d\Psi}{ds}\boldsymbol{T}.$$

Furthermore,

$$\boldsymbol{\nabla}\boldsymbol{T} = \frac{\kappa\cos\vartheta}{1 - \kappa\xi\cos\vartheta}\boldsymbol{e}_\xi \otimes \boldsymbol{T} - \frac{\kappa\sin\vartheta}{1 - \kappa\xi\cos\vartheta}\boldsymbol{e}_\vartheta \otimes \boldsymbol{T},$$

$$\boldsymbol{\nabla}\boldsymbol{e}_\xi = -\frac{\kappa\cos\vartheta}{1 - \kappa\xi\cos\vartheta}\boldsymbol{T} \otimes \boldsymbol{T} + \frac{1}{\xi}\boldsymbol{e}_\vartheta \otimes \boldsymbol{e}_\vartheta,$$

$$\boldsymbol{\nabla}\boldsymbol{e}_\vartheta = \frac{\kappa\sin\vartheta}{1 - \kappa\xi\cos\vartheta}\boldsymbol{T} \otimes \boldsymbol{T} - \frac{1}{\xi}\boldsymbol{e}_\xi \otimes \boldsymbol{e}_\vartheta,$$

$$\boldsymbol{\nabla}\boldsymbol{B} = \frac{\tau}{1 - \kappa\xi\cos\vartheta}\boldsymbol{N} \otimes \boldsymbol{T},$$

$$\boldsymbol{\nabla}\boldsymbol{N} = -\frac{\kappa}{1 - \kappa\xi\cos\vartheta}\boldsymbol{T} \otimes \boldsymbol{T} - \frac{\tau}{1 - \kappa\xi\cos\vartheta}\boldsymbol{B} \otimes \boldsymbol{T}.$$

The volume element in Ω is given by $dv = \xi|1 - \kappa\xi\cos\vartheta|ds\,d\xi\,d\vartheta$, so that the curvilinear coordinate system (s,ξ,ϑ) is well defined as long as $|1 - \kappa\xi| > 0$, which implies $\kappa(s)r < 1$ for all $s \in [0,\ell]$, since κ is non-negative by construction. The volume of Ω is

$$\mathcal{V}(\Omega) = \int_0^\ell ds \int_0^r d\xi \int_0^{2\pi} d\vartheta\,\xi(1 - \kappa\xi\cos\vartheta) = \pi r^2\ell.$$

[1] M. W. Moon, H. M. Jensen, J. W. Hutchinson, K. H. Oha, and A. G. Evans, J. Mech. Phys. Solids **50**, 2355 (2002).
[2] A. Jákli, Ch. Lischka, W. Weissflog, G. Pelzl, and A. Saupe, Liq. Cryst. **27**, 1405 (2000).
[3] A. Jákli, D. Krüerke, and G. G. Nair, Phys. Rev. E **67**, 051702 (2003).
[4] D. A. Coleman, J. Fernsler, N. Chattham, M. Nakata, Y. Takanishi, E. Korblova, D. R. Link, R.-F. Shao, W. G. Jang, J. E. McLennan, O. Mondainn-Monval, C. Boyer, W. Weissflog, G. Pelzl, L.-C. Chien, J. Zasadzinski, J. Watanabe, D. M. Walba, H. Takezoe, and N. A. Clark, Science **301**, 1204 (2003).
[5] D. J. Photinos and E. T. Samulski, Science **270**, 783 (1995).
[6] A. F. Terzis, D. J. Photinos, and E. T. Samulski, J. Chem. Phys. **107**, 4061 (1997).
[7] T. Niori, T. Sekine, J. Watanabe, T. Furukawa, and H. Takezoe, J. Mater. Chem. **6**, 1231 (1996).
[8] D. R. Link, G. Natale, R. Shao, J. E. Maclennan, N. A. Clark, E. Körblova, and D. M. Walba, Science **278**, 1924 (1997).
[9] L. Radzihovsky and T. C. Lubensky, Europhys. Lett. **54**, 206 (2001).
[10] S. T. Lagerwall, *Ferroelectric and Antiferroelectric Liquid Crystals* (Wiley-VCH, New York, 1999).
[11] P. G. de Gennes and J. Prost, *The Physics of Liquid Crystals*, 2nd ed. (Oxford University Press, Oxford, 1993).
[12] M. C. Calderer and C. Liu, Int. J. Eng. Sci. **38**, 1113 (2000).
[13] P. Bauman, M. C. Calderer, C. Liu, and D. Phillips, Arch. Ration. Mech. Anal. **165**, 161 (2002).
[14] J. Chen and T. C. Lubensky, Phys. Rev. A **14**, 1202 (1976).
[15] A. Jákli, D. Krüerke, H. Sawade, and G. Heppke, Phys. Rev. Lett. **86**, 5715 (2001).
[16] R. Memmer, Liq. Cryst. **29**, 483 (2002).
[17] L. Longa, D. Monselesan, and H. R. Trebin, Liq. Cryst. **2**, 769 (1987).
[18] A. V. Zakharov and R. Y. Dong, Phys. Rev. E **64**, 042701 (2001).
[19] I. M. Syed and C. Rosenblatt, Phys. Rev. E **67**, 041707 (2003).
[20] G. Pelzl, S. Diele, A. Jákli, Ch. Lischka, I. Wirth, and W. Weissflog, Liq. Cryst. **26**, 135 (1999).
[21] R. Amaranatha Reddy and B. K. Sadashiva, Liq. Cryst. **30**, 273 (2003).
[22] H. N. Shreenivasa Murthy and B. K. Sadashiva, J. Mater. Chem. **13**, 2863 (2003).
[23] R. A. Sones, R. G.Petschek, D. W.Cronin and E. M. Terentjev, Phys. Rev. E **53**, 3611 (1996).